applied sciences

MDPI

Article

Localized Resonance Mechanism of Rail Corrugation and Active Suppression via Wheel–Rail Self-Grinding on Urban Express Line with Different Tracks

Jie Zhong [1], Jing Tong [2,*], Chunqiang Shao [1], Chaozhi Ma [2,*] and Peng Zhou [2]

[1] China Academy of Railway Sciences (Shenzhen) Research and Design Institute Co., Ltd., Shenzhen 518000, China; tkyszzj@163.com (J.Z.); scq0920@126.com (C.S.)
[2] School of Mechanics and Civil Engineering, China University of Mining and Technology, Xuzhou 221116, China; 6208@cumt.edu.cn
* Correspondence: ts24030105a31@cumt.edu.cn (J.T.); czma@cumt.edu.cn (C.M.); Tel.: +86-13812355210 (J.T.)

Abstract

The occurrence of short-wave corrugation with wavelengths of 32–44 mm on curved sections of urban express railway lines is particularly pronounced, yet the underlying initiation mechanisms have remained insufficiently understood. Furthermore, conventional mitigation strategies—including the installation of rail dampers and passive grinding—entail substantial maintenance expenditures, thereby hindering their large-scale application. To elucidate the initiation mechanisms of rail corrugation and to formulate effective control measures, the characteristic corrugation parameters under various track structure configurations across an entire alignment were first measured and systematically analyzed. Dynamic interaction models between vehicles and three distinct track typologies were subsequently developed, together with a comprehensive analytical framework for corrugation evolution. The wheel–rail dynamic response characteristics and corrugation growth rates corresponding to each track type were examined, and the wheel–rail coupled vibration modes that exacerbate corrugation propagation in urban express lines were identified. The instantaneous wear behavior of the rail under differing creep regimes was also investigated, leading to the proposal of a novel self-mitigating approach for rail corrugation. The results demonstrate that the excitation frequency of rail corrugation is predominantly confined to the 600–700 Hz range, exhibiting a fixed-frequency characteristic that remains invariant with respect to curve radius, track structure type, and operational speed. An interesting finding is that, although the intrinsic vibration properties of different track structures diverge significantly, the third-order bending resonance of the rail segment situated between bogie wheels is largely unaffected by track-borne vibrations and manifests as a localized wheel–rail resonance within the vehicle–track coupled system. This particular resonance markedly accelerates corrugation development and is identified as the critical governing factor for corrugation initiation in urban express lines, regardless of the underlying track configuration. Furthermore, rail instantaneous wear displays a substantial phase shift under varying creep conditions, with the wear profiles under creep saturation (full sliding) and low creep (rolling–sliding) exhibiting a distinct anti-phase relationship. This insight underpins a novel self-wear suppression strategy: by intentionally mixing rolling–sliding and full-sliding operational regimes, destructive interference between the out-of-phase wear contributions is achieved, resulting in a considerably attenuated corrugation growth rate compared with exclusive rolling–sliding operation. This methodology thus offers a promising and fundamentally new alternative for the long-term management of rail corrugation through intrinsic wheel–rail interaction.

Check for updates

Academic Editor: Ephraim Suhir

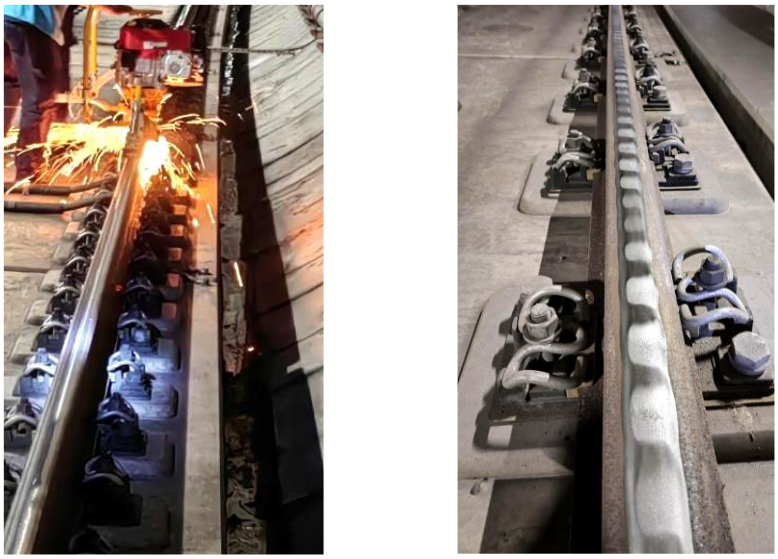
Received: 26 March 2026
Revised: 4 May 2026
Accepted: 6 May 2026
Published: 8 May 2026

Copyright: © 2026 by the authors. Licensee MDPI, Basel, Switzerland. This article is an open access article distributed under the terms and conditions of the Creative Commons Attribution (CC BY) license.

Keywords: rail corrugation; active suppression; interference cancellation; urban express line; wheel–rail coupled resonance; creeping state

1. Introduction

In contrast to conventional metro systems, urban express lines are characterized by considerably higher operational speeds and correspondingly more stringent requirements for maintenance and infrastructure integrity. To accommodate the constraints imposed by existing urban layouts on alignment design, urban express lines typically exhibit a substantial proportion of curved track, with curved segments accounting for approximately 30% to 50% of the total route length in certain cases. Field investigations conducted on a municipal express line have revealed that severe rail corrugation has developed over the majority of small-radius curved sections, with corrugation wavelengths predominantly ranging from 32 to 44 mm and a relatively rapid propagation rate, as illustrated in Figure 1. This phenomenon markedly intensifies the wheel–rail dynamic interaction and constitutes the principal cause of ancillary defects including the elastic fracture of fasteners, fatigue-induced failure at the root of T-bolts, and excessive in-cabin noise levels. Consequently, elucidating the formation mechanism of this specific category of rail corrugation and formulating effective countermeasures are essential prerequisites for ensuring both the operational safety and environmental sustainability of urban express lines.



(**a**) Just after grinding (**b**) After three months of operation

Figure 1. Rail corrugation morphology on urban express line.

Extensive research has been devoted to the genesis of rail corrugation. Jin Xuesong [1], Zhu Haiyan [2], and Grassie [3] have comprehensively reviewed the causative mechanisms, attributing corrugation primarily to self-excited or resonance-induced vibration phenomena. Friction-induced self-excited vibration has been demonstrated to be particularly pertinent in the analysis of corrugation initiation on sharp curves with radii less than 350 m [4,5]. With regard to resonance-driven mechanisms, the pinned–pinned resonance of the rail has been identified as a significant factor in the formation of short-wavelength corrugation [6,7], whereas vertical or anti-phase resonances of the track structure have been established as the direct causative agents for corrugation on tracks incorporating trapezoidal sleeper damping, elastic booted sleepers, and resilient fastening systems [8–11]. Extending these

findings, Wang Menghan and Wang Anbin [12] examined the generation of 30–40 mm wavelength corrugation on tangent track sections equipped with Cologne egg fasteners at a speed of 80 km/h, concluding that it is predominantly associated with high-frequency intrinsic vibrations of the wheel–rail coupled system. Wang Yang [13] investigated the formation of 160–200 mm wavelength corrugation on steel-spring floating slab tracks in metro applications and inferred a connection to wheel–rail P2 resonance coupled with the bending resonance of the floating slab. Furthermore, the reflection and transmission of waves between successive wheelsets [14,15] have been shown to exert a substantial influence on the development of corrugation with wavelengths of 110–160 mm in high-speed railways and 20–30 mm in metro systems.

Despite these significant advances, a critical knowledge gap persists concerning the initiation of the 32–44 mm corrugation observed across the diverse track structures deployed on urban express lines. Specifically, whereas prior work [12] has established the relevance of high-frequency wheel–rail coupled vibration for short-pitch corrugation, that study was confined to a single track typology (Cologne egg fasteners) and did not elucidate why the same characteristic wavelength emerges ubiquitously across fundamentally different track structures—ranging from monolithic slab beds to steel-spring floating slabs—as encountered in the present investigation. Moreover, while the role of local rail bending modes has been acknowledged, the existing literature has not systematically decoupled the relative contributions of global track dynamics (e.g., floating slab resonances) from those of localized rail segment vibrations confined between the wheels of a single bogie. Additionally, the potential for actively exploiting wheel–rail creep phase relationships to achieve the destructive interference of corrugation growth has not been explored; current mitigation strategies remain largely passive, relying on post hoc grinding or structural damping modifications that are both costly and logistically demanding.

The present study addresses these gaps through an integrated approach that combines comprehensive field diagnostics across an entire operational alignment, vehicle–track coupled dynamic modeling, and quantitative corrugation growth rate analysis. The principal novel contributions of this work are threefold: the demonstration that the excitation frequency of 32–44 mm corrugation on urban express lines is invariantly confined to the 600–700 Hz band irrespective of curve radius, operational speed, and—crucially—track structure type; the identification of the third-order bending resonance of the rail segment bounded by the bogie wheels as the dominant, localized vibration mode responsible for the rapid corrugation growth, a mode that remains largely insensitive to the vibratory characteristics of the supporting track bed; and the proposal and numerical validation of a novel self-wear suppression strategy predicated on the intentional mixing of rolling–sliding and full-sliding creep regimes, which leverages the anti-phase relationship of instantaneous wear depths to achieve destructive interference and thereby substantially attenuate the net corrugation growth rate.

To mitigate rail corrugation effectively, current remedial approaches encompass rail grinding, the optimization of structural dynamic properties, and the enhancement of material wear resistance. In the domain of rail grinding, Zhao Guotang [16] advocated for the elimination of the adverse effects associated with the decarburized layer during the pre-grinding phase of high-speed railway rails. With respect to structural vibration optimization, Mo X. [17] and Tran K.T. [18] investigated both the underlying principles and practical efficacy of rail vibration absorbers from theoretical and experimental standpoints. Regarding improvements in wear resistance, the application of friction modifiers [19,20] and surface-hardening techniques [21] has been shown to decelerate the progression of corrugation and augment wear durability. In summary, although extant measures have appreciably retarded the rate of corrugation development, strategies that seek to mod-

ify structural vibration characteristics by altering mechanical parameters or geometric dimensions necessitate extensive engineering interventions on lines already in service, thereby posing significant obstacles to widespread practical implementation. Furthermore, while such optimization may circumvent specific resonance phenomena, the dense modal spectrum inherent to track structures raises the possibility of inadvertently exciting resonance at alternative frequencies, potentially engendering the emergence of corrugation of a different wavelength. It is therefore evident that rail grinding and material enhancement represent passive control measures, entailing substantial maintenance expenditures and necessitating recurrent remedial actions, which in turn present formidable challenges for rail maintenance in contexts characterized by rapid corrugation propagation.

In light of the foregoing considerations, the present study first conducts a comprehensive field survey and inductive analysis of rail corrugation characteristics across varying track structures along an entire operational line. Based on these empirical findings, a dynamic model and analytical framework for rail corrugation in urban express lines are established. The characteristic manifestations and formative mechanisms of rail corrugation specific to urban express lines are systematically investigated, and a novel control methodology predicated on the principle of self-wear suppression through wheel–rail interaction is proposed. The overarching objective is to provide a conceptual foundation for long-term, operationally straightforward solutions to the persistent challenge of rail corrugation.

2. On-Site Characteristics of Rail Corrugation Under Different Track Types of Urban Express Line

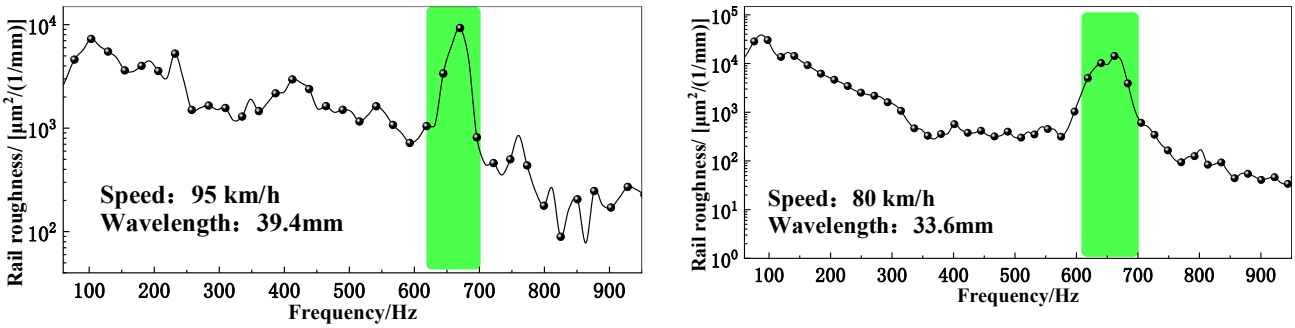
The track infrastructure of the urban express line comprises multiple structural configurations, primarily including conventional prefabricated slab track, rubber-booted floating slab track, and steel-spring floating slab track, with a uniform sleeper spacing of 60 mm. A comprehensive rail roughness survey was conducted along the entire alignment of the municipal line, identifying a total of 41 track sections exhibiting rail corrugation. Specifically, we used the measurement apparatus (CAT corrugation measuring instrument), the spatial sampling interval (2 mm), and the measurement length for each section (typically spanning 100 m per curve). The 41 sections were selected based on routine track inspection data where visual corrugation was severe and the roughness amplitude exceeded standard maintenance thresholds. Figure 2 illustrates the power spectral density (PSD) function of the rail roughness, where the pronounced energy concentration within the 600–700 Hz range characterizes the formation of rail corrugation in this frequency band. Among these identified sections, 17 segments correspond to conventional prefabricated track, 17 to rubber-booted floating slab track, and 7 to steel-spring floating slab track. The characteristic parameters of corrugation across these sections are summarized and presented in Figure 3.

As can be seen from Figure 3:

(1) Rail corrugation is exclusively localized on curved segments of the alignment, with the low (inner) rail consistently exhibiting more pronounced corrugation severity relative to the high (outer) rail. Irrespective of the curve radius, the corrugation wavelength consistently falls within the range of 32–44 mm. Based on the operational speeds recorded for vehicles traversing the corrugated sections, the corresponding excitation frequency is estimated to lie between 600 and 700 Hz. Notably, despite variations in curve radii (ranging from R550 to R1000 m) and fluctuations in vehicle running speeds (80–110 km/h) across the affected sections, the excitation frequency associated with rail corrugation remains relatively invariant.

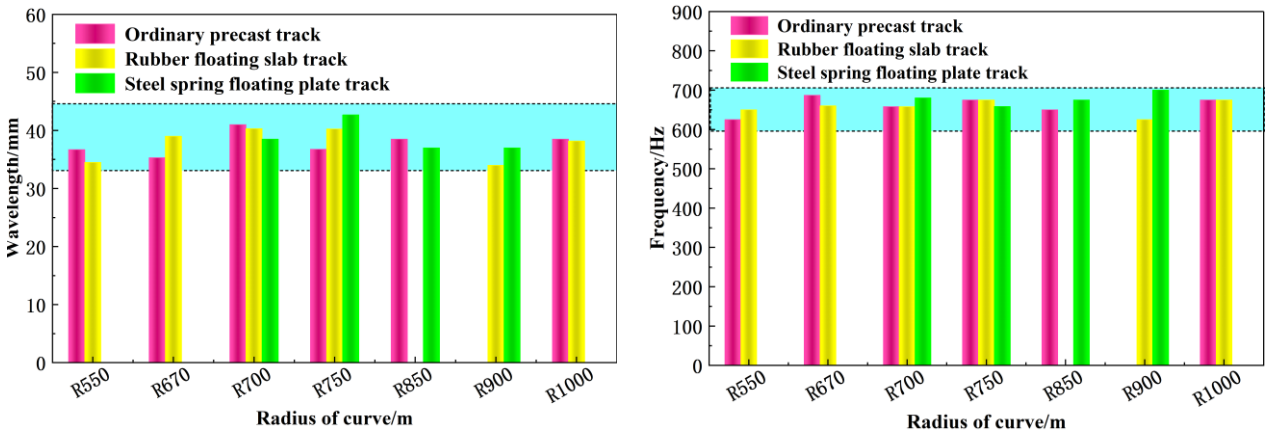
(2) Severe corrugation is observed across all track structure typologies. Although the structural configurations of conventional prefabricated track, rubber-booted floating slab

track, and steel-spring floating slab track differ substantially, the predominant excitation frequency of the resulting corrugation is essentially identical across all three systems.



(**a**) 95 km/h (**b**) 80 km/h

Figure 2. Spectrum of rail corrugation under different train speeds (The black dots in the figure denote markers representing the variations in the power spectral density for a certain segment of roughness data. The green area represents the frequency band where corrugation occurs).



(**a**) Rail corrugation wavelength (**b**) Rail corrugation excitation frequency

Figure 3. Characteristic parameters of rail corrugation under different track structures.

In summary, the rail corrugation observed on the urban express line manifests a pronounced fixed-frequency characteristic. Neither the curve radius, the track structure type, nor the vehicle operating speed exerts a substantial influence on the corrugation signature, particularly with respect to the excitation frequency. It may therefore be inferred that the corrugation phenomenon encountered in this context likely originates from natural modal resonance within the vehicle–track coupled system.

3. Analysis Model and Method of Rail Corrugation in Urban Express Line

In this section, coupled dynamic models encompassing the various track–vehicle system configurations encountered on the urban express line are established. A methodological framework for quantifying the growth rate of rail corrugation specific to urban express line operations is subsequently proposed. The validity of this analytical approach is further substantiated through comparative evaluation against in situ rail corrugation characteristics derived from field measurements.

3.1. Dynamic Interaction Model of Different Types of Vehicle–Track Coupling

In this section, a vehicle–track coupling dynamic interaction model tailored to the urban express line is developed through the integration of multibody dynamics and finite

element methods, as illustrated schematically in Figure 4. With respect to the establishment of the vehicle–track coupled dynamic interaction model, the vehicle subsystem is represented using MBD, whereas the track slab components are discretized and analyzed via FEM. The solution is obtained using the sliding window approach proposed in [14], and the distance between the vehicle extremities and the window boundaries is maintained at 60 fastener spacings. The key parameter values (stiffness and geometric dimensions) for the three distinct track types are shown in Table 1. For the rubber floating slab, the isolation pad stiffness is taken as 0.025 N/mm^3; correspondingly, the support stiffness of the steel-spring is 6.6 kN/mm.

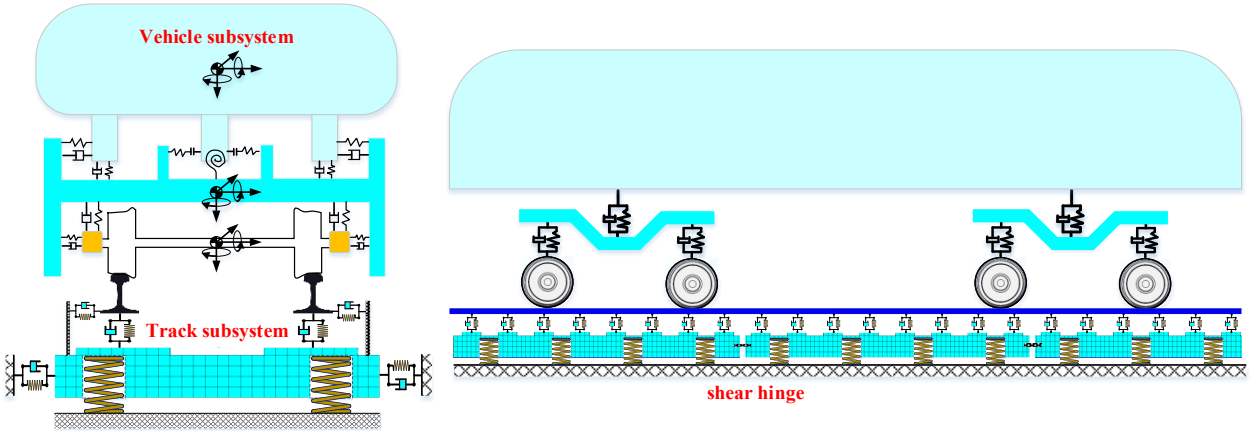


Figure 4. Vehicle–track coupling dynamic interaction model (for steel-spring floating slab track).

Table 1. Key parameters of three track types.

Track Types	Prefabricated Slab Track Bed	Rubber Floating Slab	Steel–Spring Floating Slab
Rail mass per unit length (kg)	60.64	60.64	60.64
Rail elastic modulus (GPa)	206	206	206
Rail Poisson ratio	0.3	0.3	0.3
Fasteners vertical/lateral stiffness (MN·m^{-1})	40/50	40/50	40/50
Fasteners vertical/lateral damping (kN·s·m^{-1})	30/50	30/50	30/50
Fastener node spacing (m)	0.6	0.6	0.6
Slab density (kg·m^{-3})	2500	2500	2500
Slab length (m)	4.80	4.80	4.80
Slab height (m)	0.20	0.26	0.34
Slab width (m)	2.30	2.30	2.60

The vehicle–track coupling dynamic interaction model comprises three principal subsystems: the track subsystem, the vehicle subsystem, and the wheel–rail contact subsystem [22]. The track subsystem encompasses the rail and the supporting track bed structure. The rail is modeled as a Timoshenko beam and discretized using the finite element method. Given that the fastener spacing is substantially smaller than the curve radius, the rail element length is taken as one-half of the fastener spacing, and each element is simplified as a rectilinear beam segment. Three representative track bed configurations are considered in the present analysis: the conventional prefabricated slab track bed, the rubber-booted floating slab track bed, and the steel-spring floating slab track bed. Refined finite element models are established for each track typology, from which the multi-order modal parameters are extracted (Figure 5). The governing dynamic equations of the track subsystem are

subsequently solved via the modal superposition (component mode synthesis) method. In accordance with the geometric and mechanical specifications of urban express rolling stock, the vehicle subsystem is idealized as a multibody system composed of a car body, bogie frames, wheelsets, and a series of linear/nonlinear spring-damper elements.

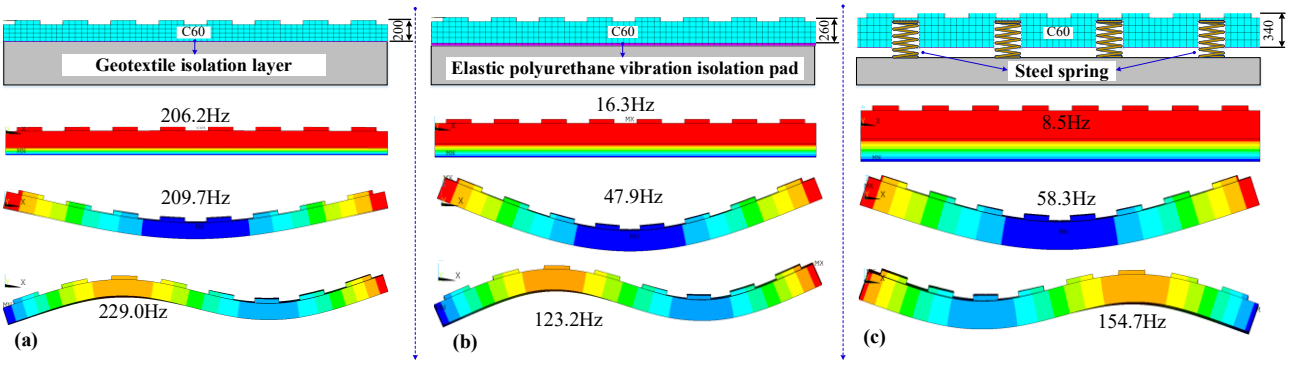


Figure 5. Vibration characteristics of different types of track beds. (**a**) Ordinary prefabricated slab track bed; (**b**) Rubber floating slab track bed; (**c**) Steel-spring floating slab track bed. (Different colors represent the relative proportional relationship of displacements at various points on the track-slab vibration modes.).

Rail corrugation on the urban express line is predominantly observed on curved sections with small radii, typically ranging from R700 to R850 m. During curve negotiation over such tight radii, the wheel flange approaches the rail gauge corner, leading to non-Hertzian wheel–rail contact conditions. To characterize the resultant wheel–rail interaction, the present study adopts the Kik–Piotrowski (K–P) method, which is predicated on the virtual penetration theory [23]. The governing dynamic equation of the complete vehicle–track coupled system is expressed in Equation (1). The wheel–rail force is calculated as shown in Equation (2).

$$\begin{bmatrix} \boldsymbol{M}_{vv} & & \\ & \boldsymbol{M}_{rr} & \\ & & \boldsymbol{M}_{ss} \end{bmatrix} \begin{bmatrix} \ddot{\boldsymbol{q}}_v \\ \ddot{\boldsymbol{q}}_r \\ \ddot{\boldsymbol{q}}_s \end{bmatrix} + \begin{bmatrix} \boldsymbol{C}_{vv} & & \\ & \boldsymbol{C}_{rr} & \boldsymbol{C}_{rs} \\ & \boldsymbol{C}_{sr} & \boldsymbol{C}_{ss} \end{bmatrix} \begin{bmatrix} \dot{\boldsymbol{q}}_v \\ \dot{\boldsymbol{q}}_r \\ \dot{\boldsymbol{q}}_s \end{bmatrix} + \begin{bmatrix} \boldsymbol{K}_{vv} & & \\ & \boldsymbol{K}_{rr} & \boldsymbol{K}_{rs} \\ & \boldsymbol{K}_{sr} & \boldsymbol{K}_{ss} \end{bmatrix} \begin{bmatrix} \boldsymbol{q}_v \\ \boldsymbol{q}_r \\ \boldsymbol{q}_s \end{bmatrix} = \begin{bmatrix} \boldsymbol{Q}_{wr} + \boldsymbol{Q}_{inv} \\ \boldsymbol{Q}_{rw} \\ 0 \end{bmatrix} \tag{1}$$

where $\boldsymbol{M}_{vv}$, $\boldsymbol{M}_{rr}$ and $\boldsymbol{M}_{ss}$ are the mass matrices of vehicle, rail, and ballast bed respectively; $\boldsymbol{C}_{vv}$, $\boldsymbol{C}_{rr}$ and $\boldsymbol{C}_{ss}$ represent the damping matrices of vehicles, rails, and ballast beds; $\boldsymbol{K}_{vv}$, $\boldsymbol{K}_{rr}$ and $\boldsymbol{K}_{ss}$ represent the stiffness matrices of vehicles, rails, and ballast beds; $\boldsymbol{C}_{rs}$ and $\boldsymbol{K}_{rs}$ are the damping and stiffness matrixes provided by the fastener; $\boldsymbol{Q}_{wr}$ and $\boldsymbol{Q}_{rw}$ represent the wheel–rail force vectors acting on the vehicle and the track respectively; $\boldsymbol{Q}_{inv}$ is the self-gravity of the vehicle.

$$N = \frac{\pi E \delta}{2(1-\mu^2)} \left[\int_{y_r}^{y_l} \int_{-x_l}^{x_l} \frac{\sqrt{x_l^2(y) - x^2}}{\sqrt{x^2 + y^2}} dxdy \right]^{-1} \int_{y_r}^{y_l} \int_{-x_l}^{x_l} \sqrt{x_l^2(y) - x^2} dxdy \tag{2}$$

where δ is the virtual penetration coefficient. E and μ are Young's modulus and Poisson's ratio, respectively. x_l, y_l, and y_r define the boundaries of the contact patch, respectively.

3.2. Analysis Process of Rail Corrugation Based on the Growth Rate Index of Corrugation

The growth rate of rail corrugation serves as a quantitative metric for assessing the severity of corrugation initiation and progression. The authors put forward this index in the context of prior investigations into the causative mechanisms underlying rail corrugation in high-speed railway applications [14]. Building upon this foundational concept, the present study incorporates the cumulative and coherent contributions of successive wheelsets

to the wear evolution at a given rail position, thereby establishing a refined analytical methodology for rail corrugation assessment specific to urban express lines. The procedural framework is schematically depicted in Figure 6 and encompasses the following four sequential steps: firstly, the dynamic response of each individual wheelset as it traverses the track is computed utilizing the vehicle–track coupled dynamic interaction model described in Section 3.1; secondly, the instantaneous wear depth induced by a single passage of multiple wheelsets over the rail is subsequently determined based on the frictional work (wear work) model; thirdly, the updated rail surface roughness profile resulting from the cumulative wear increment is derived; finally, a comparative analysis between the initial rail roughness profile and the worn roughness profile is conducted, yielding a quantitative index that characterizes the corrugation growth rate.

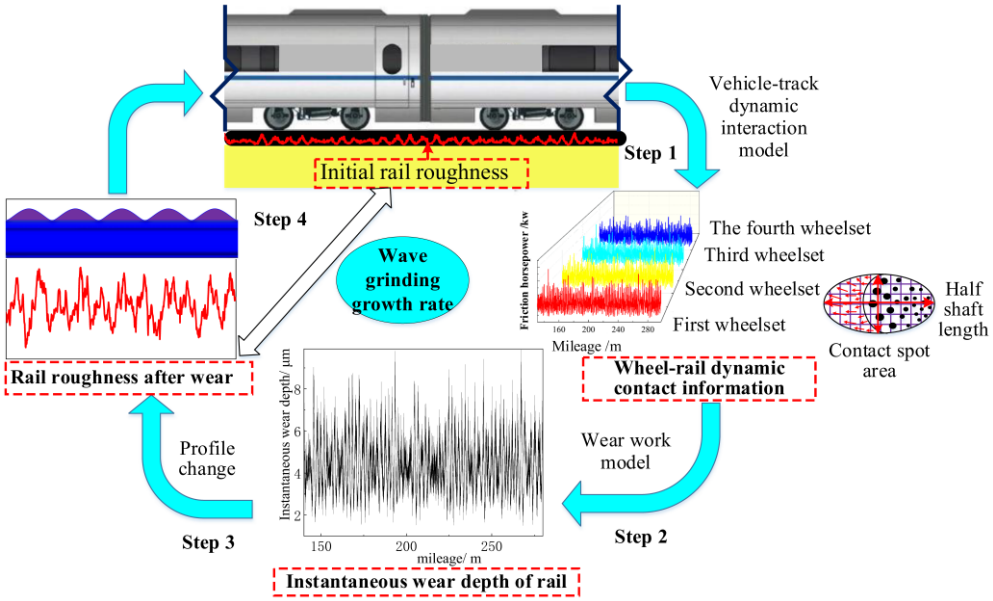


Figure 6. Analysis process of rail corrugation.

According to the wear work model [24] $\Delta \dot{m}_{\text{wear}} = C_w \cdot E_{\text{wear}} / A_c$, the instantaneous wear depth of a single wheel acting on a point on the rail tread is as follows:

$$\Delta z^k(x) = \frac{\Delta \dot{m}^k_{wear}}{\rho} \cdot \Delta t^k = \frac{C_w}{\rho} \cdot \frac{E^k_{wear}}{A^k_c} \cdot \frac{2a^k}{V^k_c} \tag{3}$$

In the formula, the superscript symbol k indicates the number of the wheelset; $\Delta z^k(x)$ represents the instantaneous wear depth of the rail tread caused by the k-th wheel; $\Delta \dot{m}_{wear}$ stands for mass wear rate; E_{wear} is wear work; C_w and ρ are wear proportional coefficient and rail material density; Δt^k represents the time when the contact spot between the k-th wheel and the rail passes through a specific point of the rail; A_c, a and V_c are the contact spot area, the half-axis length in the rolling direction, and the running speed.

Considering the cumulative influence of eight wheels of two vehicles on rail wear, the instantaneous wear depth of a point on the rail tread after each vehicle passes is expressed as follows:

$$Z_i(x) = Z_{i-1}(x) - R \sum_{k=1}^{8} \left[\Delta z^k(x) \right] \tag{4}$$

where $Z_i(x)$ is the roughness of the rail tread after the vehicle passes the i-th time; R represents the amplification factor of the iterative simulation of wear, that is, it is considered that the wear of rail in urban express lines shows a linear accumulation trend in a short cycle interval (considering the calculation cost, this paper chooses the total operating vehicle

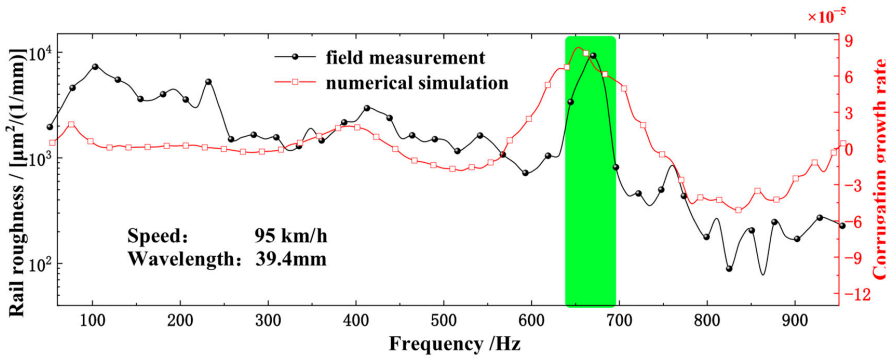
for 2 days). The rationality of this law is confirmed by the wear evolution analysis in reference [25].

As the evolution of rail roughness changes approximately exponentially during the whole grinding cycle, the wave grinding growth rate G_{cor} is defined as follows:

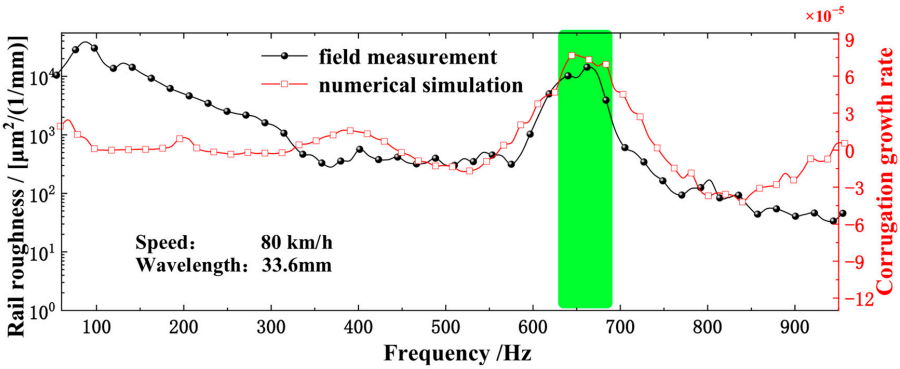
$$G_{cor} = \frac{1}{n} \ln \left[\frac{\widetilde{Z}_n(\lambda_{cor})}{\widetilde{Z}_0(\lambda_{cor})} \right] \tag{5}$$

In the formula, $\widetilde{Z}_n(\lambda_{cor})$ and $\widetilde{Z}_0(\lambda_{cor})$ respectively represent the linear self-power spectrum of rail roughness at the wavelength λ_{cor} after n wear iterations and initial wear iterations. When $G_{cor} > 0$, it means that the roughness develops and the greater its value, the easier it is to form corrugation; When $G_{cor} < 0$, it means that the roughness is suppressed.

The proposed corrugation growth rate index is subjected to verification, with particular emphasis placed on evaluating the fidelity of its predicted corrugation wavelength—a parameter of critical importance. A comparative analysis between field measurement data and numerical simulation results is presented in Figure 7. As illustrated, a greater corrugation growth rate characterizes a more rapid progression of rail roughness. It can thus be inferred that the wavelength corresponding to the peak corrugation growth rate represents the specific wavelength most susceptible to corrugation initiation. This simulation result demonstrates strong consistency with the measured values. Specifically, the findings indicate that for train operating speeds of 95 km/h and 80 km/h, the simulated corrugation wavelengths are approximately 39 mm and 34 mm, respectively, whereas the corresponding field-measured values are approximately 34 mm under the latter condition. Notably, the simulated and in situ wavelength parameters exhibit close agreement across differing operational velocities, thereby corroborating the validity of both the analytical methodology for rail corrugation tendency assessment and the associated wavelength prediction.



(**a**) Speed 95 km/h



(**b**) Speed 80 km/h

Figure 7. Verification of characteristic parameters of rail corrugation (The green area represents the frequency band where corrugation occurs).

4. Characteristics and Genesis of Rail Corrugation in Urban Express Line

Since the formation of rail corrugation originates from the intrinsic vibration characteristics of the wheel–rail coupled system, approaches such as the installation of rail dampers, while capable of mitigating such coupled resonance to a certain extent, invariably entail substantial increases in both operational maintenance costs and labor demands. In light of this constraint, the present section first delineates the underlying principle of achieving the self-wear suppression of rail corrugation through creep regulation. Subsequently, the corrugation suppression efficacy of the proposed methodology is assessed via numerical simulation, thereby furnishing a novel conceptual framework for the remediation of rail corrugation in urban express lines.

4.1. Analysis of Wheel–Rail Dynamic Response and Wave Grinding Growth Rate Under Different Rail Types

The wheel–rail dynamic response corresponding to vehicle operation over the circular curve section is extracted and presented in Figure 8. Specifically, this figure illustrates the power spectral density (PSD) curve of the wheel–rail force, characterizing the intensity distribution of the signal across the frequency domain. As illustrated in Figure 8, variations in track structure typology induce pronounced alterations in the low-frequency wheel–rail dynamic response below 200 Hz, whereas their influence on the high-frequency response remains comparatively marginal. In addition, as the frequency increases, the energy of the wheel–rail force decreases significantly. The maximum wheel–rail force energy occurs within the 40–80 Hz range, reaching 1.1 kN^2/Hz; conversely, in the high-frequency band (above 200 Hz), the energy reaches a peak near 650 Hz with a value of 0.018 kN^2/Hz.

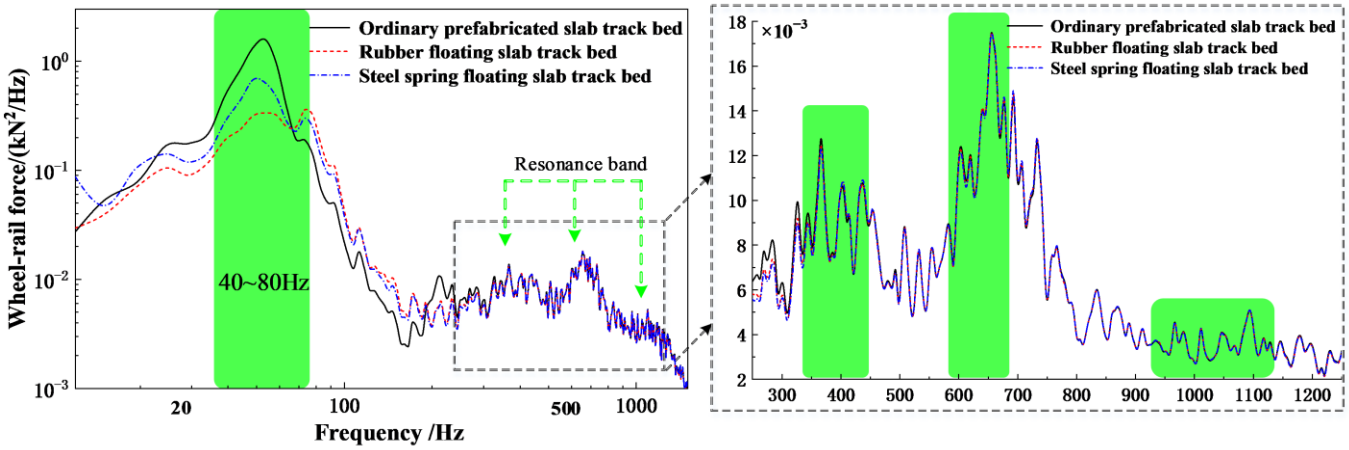


Figure 8. Wheel–rail dynamic response under different track types (Green areas represent typical resonance frequency bands).

The wheel–rail vertical force under the dynamic interaction of various track–vehicle system configurations consistently exhibits four distinct resonance peaks, with the corresponding resonance frequencies centered predominantly in the vicinity of 60 Hz, 400 Hz, 650 Hz, and 1050 Hz. It is inferred that these resonance phenomena are principally governed by wheel–rail coupled vibrations, whereas the contribution of ballastless track bed structural vibrations remains relatively inconsequential.

Subsequently, following the rail corrugation analysis procedure outlined in Section 3.2, the corrugation growth rate for the urban express line is derived and presented in Figure 9. As evident from Figure 9, within the frequency bands coinciding with the wheel–rail vertical force resonances, the rail corrugation growth rate exhibits pronounced peaks, signifying the accelerated development of rail surface roughness at these specific frequencies. Notably,

the growth rate attains its maximum value precisely at the 650 Hz vertical force resonance frequency, indicating that this particular resonance constitutes the most potent catalyst for corrugation initiation. These findings substantiate that wheel–rail resonance represents the fundamental causative factor underlying rail corrugation in urban express lines, thereby underscoring the critical importance of identifying the specific vehicle–track system modes responsible for such resonance in elucidating the corrugation genesis. Furthermore, while the corrugation growth rates associated with steel-spring and rubber-booted floating slab tracks are marginally higher than those observed for conventional prefabricated slab track, the discrepancy remains statistically insignificant.

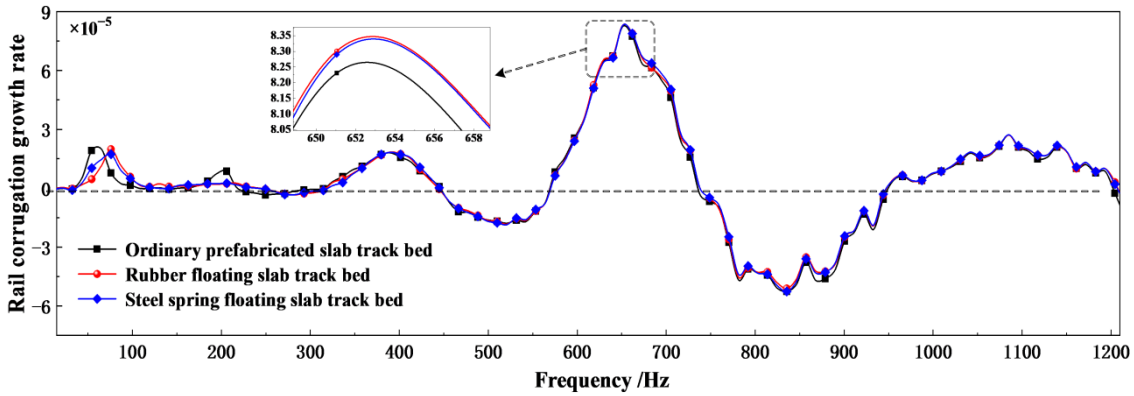


Figure 9. Rail corrugation growth rate under different track types.

4.2. Wheel–Rail Coupling Vibration Modes and Rail Corrugation Causes Under Different Rail Types

The modal characteristics of the wheel–rail coupled vibration across different track typologies were investigated through finite element modal analysis incorporating the coupled interaction between the track structure and the wheelset. The corresponding results are summarized in Table 2.

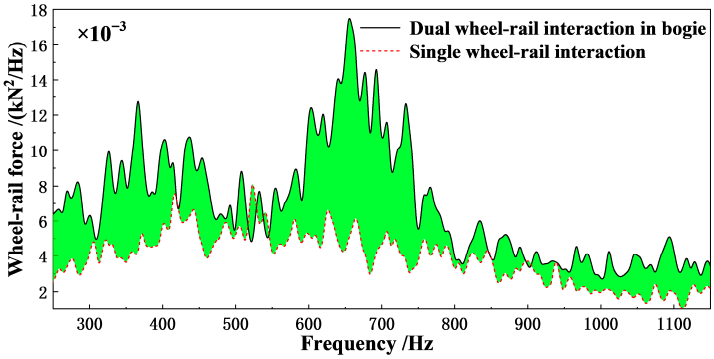
Table 2. Wheel–rail coupled vibration modes under different track structure types.

Modal Type	Ordinary Prefabricated Slab Track Bed	Rubber Floating Slab Track Bed	Steel–Spring Floating Slab Track Bed
Wheel–rail P2 resonance	wheel, railway rail, 55.9Hz, roadbed	73.3Hz	53.8Hz
Second-order bending of rail	383.9Hz	385.5Hz	380.9Hz
Third-order bending of rail	660.1Hz	660.3Hz	661.8Hz
Pinned–pinned vibration of rail	966.9Hz	966.9Hz	966.9Hz

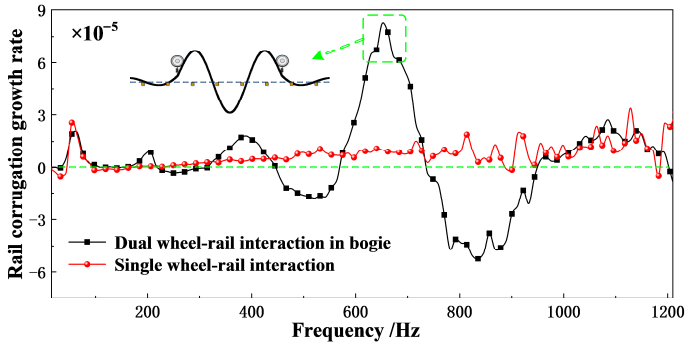
It can be found from Table 1 that the P2 resonance mode of wheel–rail and the frequencies of the second-order bending, third-order bending and pinned–pinned vibration modes of the rail between bogie wheels match the resonance frequency of the wheel–rail

dynamic response in Figure 8, respectively, and it is inferred that these four wheel–rail coupling vibration modes are the dominant contributing factors to induce the resonance of the wheel–rail system. Further analysis shows that the vibration mode and frequency of the P2 resonance mode of wheel–rail systems are significantly different under different track structures, and this mode of wheel–rail system presents the global coupled vibration property of its associated structure, in which the anti-phase bending of the rubber floating slab track bed and the in-phase bending of the steel-spring floating slab track bed increase and decrease this P2 resonance mode frequency respectively. The second-order bending, third-order bending, and pinned–pinned vibration modes and modes of the rail between bogie wheels are relatively less affected by the ballast structure type, showing their own local vibration properties, which is the internal reason why the high-frequency wheel–rail dynamic resonance is not significantly affected by the ballast vibration.

Figure 10 further compares the wheel–rail force and rail corrugation growth rate under the action of single wheel and bogie double wheels, and there is a significant difference between them. Specifically, the resonance peak of wheel–rail force disappears under the action of a single wheel, and the growth rate of rail corrugation is also greatly reduced, which is significantly different from the results under the action of bogie double wheels. Furthermore, we elaborated on the physical mechanism underpinning this phenomenon: the two wheels of a bogie effectively act as dynamic boundary conditions (pinning points), creating a confined vibratory subsystem in the rail segment between them. Wave transmission and reflection along the rail between double wheelsets will occur. This specific boundary condition is what enables the excitation of the third-order bending resonance at 600–700 Hz. When the second wheel is removed in the single-wheel model, this confined boundary condition vanishes, and consequently, the localized resonance is suppressed. As there is no local bending vibration mode of the rail between bogie wheels under the action of a single wheel, it is proved from the side that the local bending resonance of the rail between bogie wheels is an important reason for the formation of rail corrugation in urban express lines.



(**a**) Influence of local rail bending vibration between bogie wheels on wheel–rail force



(**b**) Influence of local rail bending vibration between bogie wheels on rail corrugation growth rate

Figure 10. Influence of local rail bending vibration between bogie wheels on wheel–rail force and rail corrugation growth rate.

Generally speaking, steel-spring floating slab track, rubber cushion floating slab track, and ordinary ballast bed are typical track structures used in the city express line, and there are significant differences in structural form and vibration characteristics, but their wave wear phenomena are mainly due to the third-order bending resonance of the rails between bogie wheels. The resonance is less affected by the vibration of the ballast bed structure, and it shows a typical wheel–rail local resonance property in the vehicle-rail strong coupling system. Therefore, the characteristic parameters (excitation frequency) of the three types of track display wave grinding are basically the same. In addition, different from the analysis results of the rail corrugation of high-speed railways in reference [14], the high-speed railway with a speed of 300 km/h has a significant corrugation at the pinned–pinned resonance of the rail near 1000 Hz, but the fretting growth rate of the rail of the urban express line is small at this resonance frequency, and the fretting characteristics are not obvious. This is mainly due to the low running speed of the urban express line and the small impact energy of the wheel and rail, as stimulating the pinned–pinned resonance of the rail around 1000 Hz requires higher energy input.

5. A New Method for Restraining Rail Corrugation Self-Wear Based on Creep Control

Since the formation of rail corrugation originates from the intrinsic vibration characteristics of the wheel–rail coupled system, mitigation strategies such as the installation of rail dampers, while capable of attenuating the coupled resonance to some degree, invariably incur substantial increases in maintenance expenditures and labor requirements. Considering this limitation, the present section first delineates the underlying principle of the self-wear suppression of rail corrugation achieved through creep regulation. Subsequently, the efficacy of the proposed methodology in mitigating corrugation development is evaluated via numerical simulation, thereby furnishing a novel conceptual framework for the remediation of rail corrugation in urban express lines.

5.1. Principle of Restraining Rail Wave Wear by Wheel–Rail Natural Wear

A single harmonic excitation with a wavelength of 40 mm and a depth of 80 μm was imposed within the vehicle–track coupled dynamic interaction model, and the wheel–rail creep is set to two states, namely, small creep and saturation, and the instantaneous wear depth of the rail under these two creep states is obtained by simulation, as shown in Figure 11.

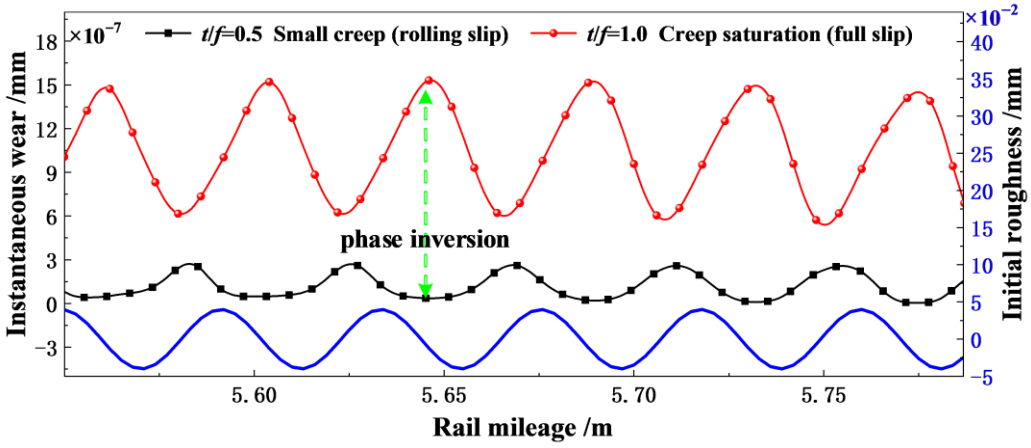


Figure 11. Influence of wheel–rail creep on rail instantaneous wear (t is the adhesion coefficient, f is the wheel–rail friction coefficient).

From Figure 11, it can be found that the greater the wheel–rail creep, the higher the instantaneous rail wear when the train passes by. The instantaneous wear phase of the rail is different under different creep conditions, and the phase difference in the instantaneous wear of a rail under creep saturation (full sliding) and small creep (rolling–sliding) is close to 180, showing the law of anti-phase. It can be seen that the different creep states between wheel and rail will cause the instantaneous wear phase shift in the rail. According to the principle of wave superposition, the instantaneous rail wear caused by multi-train excitation shows a significant interference cancellation phenomenon under different wheel–rail creep conditions. This phenomenon is similar to the interference effect in classical wave theory: light intensity attenuation caused by optical interference and noise suppression caused by acoustic interference. The closer the phase difference between two waves at the interference point is to the opposite phase, the better the interference cancellation effect is. Based on this, the principle of the wheel–rail self-wear suppression of the rail corrugation is put forward, that is, the instantaneous wear phase of the wheel–rail is shifted by running trains in different creep states, and the cumulative rate of rail corrugation is slowed down by interference cancellation which suppresses the formation of rail corrugation. It is worth noting that interference cancellation is used here strictly as a conceptual and phenomenological analogy to aid understanding, rather than a strict physical equivalence.

Based on this, a wheel–rail self-wear suppression strategy for mitigating rail corrugation on curved sections of urban express lines is proposed, as shown in Figure 12. According to the characteristics of rail corrugation, the creep state of train wheels and rails is dynamically adjusted to realize the interference cancellation of rail instantaneous wear under full sliding and rolling–sliding conditions. Combined with the analysis process of rail corrugation in Section 3.2, the proportion of train trips in different creep states is further analyzed, and the regulation scheme that makes the wear cancellation most significant (the increase rate of corrugation is the smallest) is determined. The regulation of different creep states of the wheel and rail can be realized by the friction regulator [19] on the rail top or the grind on the wheel tread. Furthermore, it is imperative to acknowledge the inevitable consequences of intentionally inducing such full-sliding states, namely increased rail and wheel wear, potential energy losses, and altered rolling noise. Fundamentally, this strategy represents a deliberate operational trade-off: sacrificing a degree of uniform material lifespan to prevent the severe, localized structural damage and high-impact vibrations invariably caused by rail corrugation (non-uniform wear).

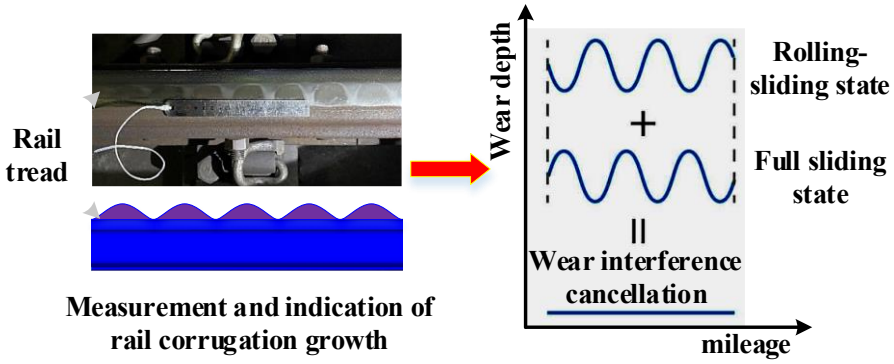


Figure 12. Rail self-grinding suppression strategy based on interference elimination.

5.2. Suppression Effect of Rail Wave Grinding Self-Polishing

This paper discusses the suppression effect of wheel–rail self-wear under the mixed operation of full sliding and rolling–sliding between wheel and rail. Two distinct wheel–rail creep states are considered: a rolling–sliding regime characterized by a friction utilization

factor of t/f = 0.5, and a full sliding regime with t/f = 1.0. By varying the proportion of train passages assigned to each creep condition, the corresponding rail corrugation growth rate is determined, as shown in Figure 13. As can be seen from Figure 13, the growth rate of rail corrugation in rolling–sliding and full-sliding mixed operation is greatly reduced compared with that in a single rolling–sliding state, which shows that the train can act as a "grinding car" in full-sliding state by regulating and controlling the wheel–rail creep state of a certain line, which has a positive effect on the control of rail corrugation.

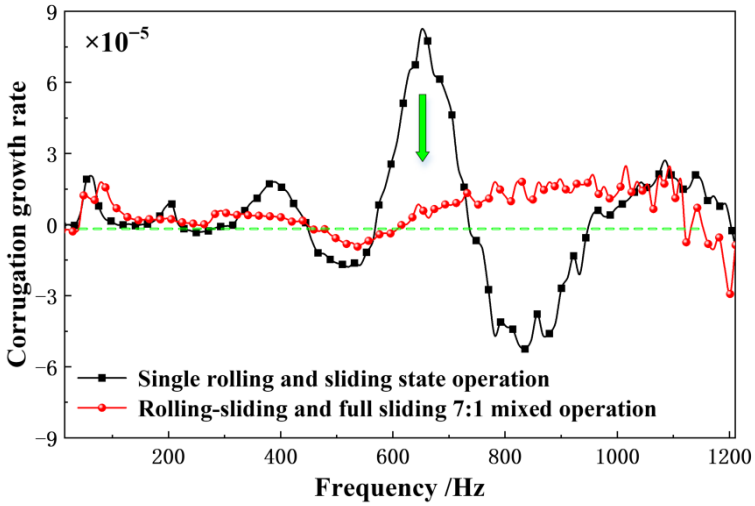
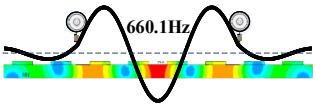
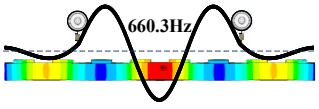
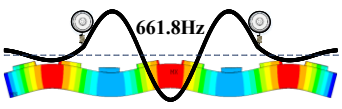


Figure 13. Self-grinding suppression effect based on wheel–rail creep control.

This study aims to propose an innovative maintenance-free idea for the long-term treatment of rail corrugation. Different from the traditional friction management method of uniform coating, the friction coefficient of the wheel–rail interface is actively regulated through the selective and precise spraying of rail friction improver, or installing or optimizing on-board tread grinding subsystems on key trains during a specific period of time or when some trains pass, creating a mixed train running state of "rolling–sliding" and "full sliding". Admittedly, the practical implementation of this method necessitates further comprehensive investigation into the quantitative relationship between the application of friction modifiers and the precise regulation of wheel–rail creep states. These critical aspects will serve as the primary focus of our subsequent research. The characteristics, causes, and control measures of rail corrugation under different track types are shown in Table 3.

Table 3. Characteristics, causes, and control measures of rail corrugation under different track types.

Track Type	Field Corrugation Characteristics	Dominant Contributing Factors	Possible Control Measures
Ordinary prefabricated slab track bed	Wavelength: 32–44 mm Excitation frequency: 600–700 Hz	 Rail third-order bending resonance	Achieving rail self-grinding by mixing rolling–sliding and full-sliding
Rubber floating slab track bed	Wavelength: 32–44 mm Excitation frequency: 600–700 Hz	 Rail third-order bending resonance	
Steel–spring floating slab track bed	Wavelength: 32–44 mm Excitation frequency: 600–700 Hz	 Rail third-order bending resonance	

6. Conclusions

This study has systematically characterized the rail corrugation features observed across the entire alignment of an urban express line under diverse track structure configurations. A dedicated analytical framework and methodology for assessing rail corrugation specific to urban express operations have been developed, through which the underlying causative mechanisms have been elucidated. Furthermore, a novel conceptual strategy for corrugation mitigation—predicated on the active modulation of wheel–rail creep conditions—has been proposed. The principal findings and their associated scientific contributions are summarized as follows:

(1) The excitation frequency of rail corrugation on the urban express line is predominantly concentrated within the 600–700 Hz band, exhibiting a distinct and invariant fixed-frequency characteristic. Notably, parameters including curve radius, track structure typology, and vehicle operating speed exert no statistically significant influence on this dominant excitation frequency.

(2) Although the modal frequencies and mode shapes of the wheel–rail P2 resonance exhibit pronounced sensitivity to variations in track structure configuration, the second- and third-order bending modes of the rail segment situated between the bogie wheels—as well as the pinned–pinned resonance mode—demonstrate comparatively weak dependence on track bed typology. These higher-order modes are instead governed by localized vibration characteristics inherent to the rail segment itself. An interesting insight emerging from this analysis is that the third-order bending resonance of the rail confined between the bogie wheels constitutes the primary and invariant driver of corrugation initiation. This localized resonance accelerates corrugation propagation far more rapidly than global track modes and is identified as the dominant contributing factor in the formation of 600–700 Hz rail corrugation on urban express lines, irrespective of the underlying track structure.

(3) The instantaneous wear phase of the rail exhibits a pronounced dependence on the prevailing creep regime. Specifically, the wear profiles corresponding to creep saturation (full sliding) and low-creep (rolling–sliding) conditions manifest a distinct anti-phase relationship. This finding introduces a novel mechanistic basis for corrugation control: By intentionally mixing operational regimes to achieve destructive interference between these out-of-phase wear contributions, the net corrugation growth rate is substantially diminished relative to that observed under exclusive rolling–sliding operation. The results thereby demonstrate the considerable potential for achieving the effective self-wear suppression of rail corrugation through the deliberate regulation of wheel–rail creep states, a strategy that fundamentally differs from conventional passive grinding or damping interventions.

Author Contributions: Conceptualization, J.Z. and C.M.; methodology, J.Z.; software, P.Z.; validation, J.Z., J.T. and C.M.; formal analysis, C.S.; investigation, J.Z.; resources, J.Z. and C.S.; data curation, P.Z., J.T. and C.M.; writing—original draft preparation, C.M.; writing—review and editing, J.T.; visualization, C.M. and J.T. All authors have read and agreed to the published version of the manuscript.

Funding: This research was funded by the China Academy of Railway Sciences (2024SZ05) and National Natural Science Foundation of China (52308468).

Institutional Review Board Statement: Not applicable.

Informed Consent Statement: Not applicable.

Data Availability Statement: The original contributions presented in this study are included in the article. Further inquiries can be directed to the corresponding author.

Conflicts of Interest: Authors Jie Zhong and Chunqiang Shao were employed by the company "China Academy of Railway Sciences (Shenzhen) Research and Design Institute Co., Ltd., Shenzhen 518000, China". The remaining authors declare that the research was conducted in the absence of any commercial or financial relationships that could be construed as a potential conflict of interest.

References

1. Jin, X.; Li, X.; Li, W.; Wen, Z. Review of rail corrugation progress. *J. Southwest JiaoTong Univ.* **2016**, *29*, 264–273.
2. Zhu, H.; Yuan, Y.; Xiao, Q.; Li, J.; Zhen, Y. Review of rail corrugation progress. *J. Traffic Transp. Eng.* **2021**, *21*, 110–133.
3. Grassie, S.L. Rail corrugation: Characteristics, causes, and treatments. *Proc. Inst. Mech. Eng. Part F J. Rail Rapid Transit* **2009**, *223*, 581–596. [CrossRef]
4. Chen, G.; Qian, W.; Mo, J.; Zhu, M. A transient dynamics study on wear-type rail corrugation on a tight curve due to the friction-induced self-excited vibration of a wheelset-track system. *J. Mech. Eng.* **2014**, *50*, 71–76. [CrossRef]
5. Cui, X.; Chen, G.; Zhao, J.; Yan, W.; Ouyang, H. Field investigation and numerical study of the rail corrugation caused by frictional self-excited vibration. *Wear* **2017**, *376–377*, 1919–1929. [CrossRef]
6. Nielsen, J.C.O. Numerical prediction of rail roughness growth on tangent railway tracks. *J. Sound Vib.* **2003**, *267*, 537–548. [CrossRef]
7. Yu, M.; Wang, W.; Liu, J. High frequency dynamic characteristics of high-speed wheel-rail transient rolling contact in rail corrugation section. *China Railw. Sci.* **2018**, *39*, 58–66.
8. Zhang, H.; Liu, W.; Liu, W.; Wu, Z. Study on the cause and treatment of rail corrugation for Beijing metro. *Wear* **2014**, *317*, 120–128. [CrossRef]
9. Li, X.; Li, W.; Shen, Y.; Wen, Z.; Jin, X. Study on the rail corrugation of the ladder-type sleepers track based on the track vibration theory. *J. Mech. Eng.* **2016**, *52*, 121–128. [CrossRef]
10. Li, X.; Li, W.; Wu, L.; Wang, H.; Wen, Z.; Jin, X. Preliminary study on rail corrugation of rubber booted short sleepers track. *J. China Railw. Soc.* **2014**, *36*, 80–85.
11. Li, W.; Zhou, Z.; Wen, Z. Initiation cause of subway rail corrugation on track with rubber-booted short sleepers. *J. Southwest JiaoTong Univ.* **2021**, *56*, 619–626.
12. Wang, M.; Gu, X.; Wang, A. Mechanism of rail corrugation formation in straight track sections with cologne-egg fasteners. *J. Railw. Sci. Eng.* **2024**, *21*, 3595–3607.
13. Wang, Y.; Hu, J.; Xiao, H.; Cui, X.; Liu, G.; Zhang, Z. Vibration characteristics of spring-steel floating slab track and cause analysis of rail corrugation. *J. Railw. Sci. Eng.* **2023**, *20*, 2456–2466.
14. Ma, C.; Gao, L.; Xin, T.; Cai, X.; Nadakatti Mahantesh, M.; Wang, P. The dynamic resonance under multiple flexible wheelset-rail interactions and its influence on rail corrugation for high-speed railway. *J. Sound Vib.* **2021**, *498*, 115968. [CrossRef]
15. Tao, G.; Yuan, Q.; Yang, X.; Wu, X.; Xie, Q.; Guan, Q.; Li, W.; Wen, Z. On short-pitch rail corrugation of suburban express railway caused by localized rail-bending vibrations within the bogie wheelbase. *Int. J. Rail Transp.* **2025**, *13*, 1200–1218. [CrossRef]
16. Zhao, G. Several urgent problems to be solved in railway transportation system. *J. Mech. Eng.* **2018**, *54*, 1–2. [CrossRef]
17. Cui, X.; Xiao, Y.; Zhong, Y.; Li, J.; Yin, Y.; Kong, X.; Zhu, Q. Study on the effect of rail vibration absorber on the formation and evolution of rail corrugation in cologne egg fastener section of metro. *Eng. Mech.* **2024**, 1–12. Available online: https://link.cnki.net/urlid/11.2595.o3.20240918.1500.020 (accessed on 5 May 2026).
18. Liu, W.; Zhang, H.; Chen, J.; Du, L. A test of treating rail corrugation by tuned rail damper for Beijing metro. *J. Vib. Eng.* **2019**, *32*, 695–700.
19. Eadie, D.T.; Santoro, M. Top-of-rail friction control for curve noise mitigation and corrugation rate reduction. *J. Sound Vib.* **2006**, *293*, 747–757. [CrossRef]
20. Egana, J.I.; Vinolas, J.; Gil-Negrete, N. Effect of liquid high positive friction (HPF) modifier on wheel-rail contact and rail corrugation. *Tribol. Int.* **2005**, *38*, 769–774. [CrossRef]
21. Wang, P.; Liu, Y.; Gao, Y.; Xu, J.; An, B.; Guo, J. A study on influence of surface strengthening on wheel-rail rolling contact behavior at rail corrugation. *J. China Railw. Soc.* **2020**, *42*, 105–112.
22. Zhai, W.; Xia, H.; Cai, C.; Gao, M.; Li, X.; Guo, X.; Zhang, N.; Wang, K. High-speed train–track–bridge dynamic interactions–Part I: Theoretical model and numerical simulation. *Int. J. Rail Transp.* **2013**, *1*, 3–24. [CrossRef]
23. Piotrowski, J.; Kik, W. A simplified model of wheel/rail contact mechanics for non-Hertzian problems and its application in rail vehicle dynamic simulations. *Veh. Syst. Dyn.* **2008**, *46*, 27–48. [CrossRef]

24. Zobory, I. Prediction of wheel/rail profile wear. *Veh. Syst. Dyn.* **1997**, *28*, 221–259. [CrossRef]
25. Fu, B.; Bruni, S.; Luo, S. Study on wheel polygonization of a metro vehicle based on polygonal wear simulation. *Wear* **2019**, *438–439*, 203071. [CrossRef]

Disclaimer/Publisher's Note: The statements, opinions and data contained in all publications are solely those of the individual author(s) and contributor(s) and not of MDPI and/or the editor(s). MDPI and/or the editor(s) disclaim responsibility for any injury to people or property resulting from any ideas, methods, instructions or products referred to in the content.